AFRL-RX-TY-TP-2010-0031

SUPRAMOLECULAR ASSEMBLY OF A BIOMINERALIZING ANTIMICROBIAL PEPTIDE IN COARSE-GRAINED MONTE CARLO SIMULATIONS (POSTPRINT)

D. Matthew Eby
Universal Technology Corporation
1270 North Fairfield Road
Dayton, OH 45432

Glenn R. Johnson
Airbase Technologies Division
Air Force Research Laboratory
139 Barnes Drive, Suite 2
Tyndall Air Force Base, FL 32403-5323

Barry L. Farmer
Materials and Manufacturing Directorate
Air Force Research Laboratory
Wright-Patterson Air Force Base, OH 45433

Ras B. Pandey
Department of Physics and Astronomy
University of Southern Mississippi
Hattiesburg, MS 39406

Contract No. FA8650-07-D-5800-0037

July 2010

AIR FORCE RESEARCH LABORATORY
MATERIALS AND MANUFACTURING DIRECTORATE

■ **Air Force Materiel Command** ■ **United States Air Force** ■ **Tyndall Air Force Base, FL 32403-5323**

AFRL-RX-TY-TP-2010-0031

SUPRAMOLECULAR ASSEMBLY OF A BIOMINERALIZING ANTIMICROBIAL PEPTIDE IN COARSE-GRAINED MONTE CARLO SIMULATIONS (POSTPRINT)

D. Matthew Eby
Universal Technology Corporation
1270 North Fairfield Road
Dayton, OH 45432

Glenn R. Johnson
Airbase Technologies Division
Air Force Research Laboratory
139 Barnes Drive, Suite 2
Tyndall Air Force Base, FL 32403-5323

Barry L. Farmer
Materials and Manufacturing Directorate
Air Force Research Laboratory
Wright-Patterson Air Force Base, OH 45433

Ras B. Pandey
Department of Physics and Astronomy
University of Southern Mississippi
Hattiesburg, MS 39406

Contract No. FA8650-07-D-5800-0037

July 2010

AIR FORCE RESEARCH LABORATORY
MATERIALS AND MANUFACTURING DIRECTORATE

■ **Air Force Materiel Command** ■ **United States Air Force** ■ **Tyndall Air Force Base, FL 32403-5323**

REPORT DOCUMENTATION PAGE

Form Approved
OMB No. 0704-0188

PLEASE DO NOT RETURN YOUR FORM TO THE ABOVE ADDRESS.

1. REPORT DATE *(DD-MM-YYYY)*	2. REPORT TYPE	3. DATES COVERED *(From - To)*
05-JUL-2010	Journal Article - POSTPRINT	01-JUN-2009 -- 30-JUN-2010

4. TITLE AND SUBTITLE

Supramolecular Assembly of a Biomineralizing Antimicrobial Peptide in Coarse-Grained Monte Carlo Simulations (POSTPRINT)

5a. CONTRACT NUMBER

FA8650-07-D-5800-0037

5b. GRANT NUMBER

5c. PROGRAM ELEMENT NUMBER

0602102F

6. AUTHOR(S)

*Eby, D. Matthew; ^Johnson, Glenn R.; ^^Farmer, Barry L.;
**Pandey, Ras B.

5d. PROJECT NUMBER

4915

5e. TASK NUMBER

L0

5f. WORK UNIT NUMBER

Q140LA62

7. PERFORMING ORGANIZATION NAME(S) AND ADDRESS(ES)

*Universal Technology Corporation, 1270 North Fairfield Road, Dayton, OH 45432; ^^Materials and Manufacturing Directorate, Air Force Research Laboratory, Wright-Patterson Air Force Base, OH 45433; **Department of Physics and Astronomy, University of Southern Mississippi, Hattiesburg, MS 39406

8. PERFORMING ORGANIZATION REPORT NUMBER

9. SPONSORING/MONITORING AGENCY NAME(S) AND ADDRESS(ES)

^Air Force Research Laboratory
Materials and Manufacturing Directorate
Airbase Technologies Division
139 Barnes Drive, Suite 2
Tyndall Air Force Base, FL 32403-5323

10. SPONSOR/MONITOR'S ACRONYM(S)

AFRL/RXQL

11. SPONSOR/MONITOR'S REPORT NUMBER(S)

AFRL-RX-TY-TP-2010-0031

12. DISTRIBUTION/AVAILABILITY STATEMENT

Distribution Statement A: Approved for public release; distribution unlimited.

13. SUPPLEMENTARY NOTES

Distribution Code 20: JOURNAL ARTICLES; DTIC USERS ONLY. U.S. Government or Federal Purpose Rights License. Document contains color images. Published on http://pubs.rsc.org | doi:10.1039/C0CP01364A.

14. ABSTRACT

Monte Carlo simulations are used to model the self-organizing behavior of the biomineralizing peptide KSL (KKVVFKVKFK) in the presence of phosphate. Originally identified as an antimicrobial peptide, KSL also directs the formation of biosilica through a hypothetical supramolecular template that requires phosphate for assembly. Specificity of each residue and the interactions between the peptide and phosphate are considered in a coarse-grained model. Both local and global physical quantities are calculated as the constituents execute their stochastic motion in the presence and absence of phosphate. Ordered peptide aggregates develop after simulations reach thermodynamic equilibrium, wherein phosphates form bridging ligands with lysines and are found interdigitated between peptide molecules. Results demonstrate that interactions between the lysines and phosphate drive self-organization into lower energy conformations of interconnected peptide scaffolds that resemble the supramolecular structures of polypeptide- and polyamine-mediated silica condensation systems. Furthermore, the specific phosphate–peptide organization appears to mimic the zwitterionic structure of native silaffins (scaffold proteins of diatom shells), suggesting a similar template organization for silica deposition between the in vitro KSL and silaffin systems.

15. SUBJECT TERMS

antimicrobial peptide, Monte Carlo, simulation, coarse-grain, modeling, silica, supramolecular assembly

16. SECURITY CLASSIFICATION OF:			17. LIMITATION OF ABSTRACT	18. NUMBER OF PAGES	19a. NAME OF RESPONSIBLE PERSON
a. REPORT	b. ABSTRACT	c. THIS PAGE			Glenn R. Johnson
U	U	U	UU	8	19b. TELEPHONE NUMBER *(Include area code)*

Reset

Standard Form 298 (Rev. 8/98)
Prescribed by ANSI Std. Z39.18

Supramolecular assembly of a biomineralizing antimicrobial peptide in coarse-grained Monte Carlo simulations†

D. Matthew Eby,[ab] Glenn R. Johnson,[b] Barry L. Farmer[c] and Ras B. Pandey*[d]

Received 29th July 2010, Accepted 7th October 2010
DOI: 10.1039/c0cp01364a

Monte Carlo simulations are used to model the self-organizing behavior of the biomineralizing peptide KSL (KKVVFKVKFK) in the presence of phosphate. Originally identified as an antimicrobial peptide, KSL also directs the formation of biosilica through a hypothetical supramolecular template that requires phosphate for assembly. Specificity of each residue and the interactions between the peptide and phosphate are considered in a coarse-grained model. Both local and global physical quantities are calculated as the constituents execute their stochastic motion in the presence and absence of phosphate. Ordered peptide aggregates develop after simulations reach thermodynamic equilibrium, wherein phosphates form bridging ligands with lysines and are found interdigitated between peptide molecules. Results demonstrate that interactions between the lysines and phosphate drive self-organization into lower energy conformations of interconnected peptide scaffolds that resemble the supramolecular structures of polypeptide- and polyamine-mediated silica condensation systems. Furthermore, the specific phosphate–peptide organization appears to mimic the zwitterionic structure of native silaffins (scaffold proteins of diatom shells), suggesting a similar template organization for silica deposition between the *in vitro* KSL and silaffin systems.

1. Introduction

The mechanism of silica formation has been long studied in the materials sciences, where the polycondensation of silicic acid can be completed using acid–base chemistry and directed into a variety of silica structures using organic molecule mediators.[1] Similar condensation chemistry occurs in natural systems at the nanoscale and is dominated by marine microorganisms such as diatoms, radiolarian, and synurophytes.[2,3] The microbes perfected silica synthesis millions of years before us and to a level of complexity that is superior to our ability to create similar structures in the laboratory. For the materials chemist, the goal is to mimic the architecture of these biological systems for useful applications in nanotechnology.

In the past two decades, research unlocked many mysteries of diatom shell (frustle) formation. Critical discoveries revealed that the polyionic proteins (silaffins) and long-chain polyamines (LCPAs) synthesized by select diatom species are used to precipitate silica and direct its deposition into exquisite architectures.[4–6] When extracted from the frustules of diatoms, silaffins promote *in vitro* silica precipitation with silicic acid in aqueous solutions at a wide pH range.[7] Silica forms rapidly at room temperature in the absence of other ionic catalysts or cofactors (buffers, salts, and other ionic species) that are normally required with *in vitro* biosilica synthesis. The silaffins are uniquely functionalized; serine residues are phosphorylated and select lysines are posttranslationally modified with branched polyamine chains. This zwitterionic structure of the protein facilitates self-assembly into macromolecular structures, which mediates the polycondensation of silicic acid to form silica spheres *in vitro* and intricate diatom frustules *in vivo*.

Since the discovery of silaffins and LCPAs, several other unrelated proteins, synthetic peptides, and polyamines have also been shown to catalyze silica biomineralization reactions.[8,9] Synthetic and other natural, unmodified peptides that induce silica condensation share similar electrostatic properties to natural silaffins, but most require the addition of multivalent anions (*e.g.*, phosphate) and are restricted to circumneutral pH to facilitate biomineralization reactions.[10–12] The presence of phosphate and a combination of charged and uncharged amines in neutral to alkaline conditions mimic the properties of the poly-ionic modifications on native silaffins.[13,14] The zwitterionic properties facilitate intermolecular interactions and promote self-assembly into supramolecular aggregates, which has been shown to be a prerequisite for silica formation. Liquid-phase ^{31}P NMR spectroscopy of the native silaffin

[a] *Universal Technology Corporation, 139 Barnes Dr., Suite 2, Tyndall Air Force Base, FL 32403, USA. E-mail: matt.eby.ctr@tyndall.af.mil; Fax: +1 850 283 6090; Tel: +1 850 283 6026*
[b] *Microbiology and Applied Biochemistry, Materials and Manufacturing Directorate, Air Force Research Laboratory, 139 Barnes Dr., Suite 2, Tyndall AFB, FL 32403, USA. E-mail: glenn.johnson@tyndall.af.mil; Fax: +1 850 283 6090; Tel: +1 850 283 6223*
[c] *Materials and Manufacturing Directorate, Air Force Research Laboratory, Wright Patterson Air Force Base, OH 45433, USA. E-mail: barry.farmer@wpafb.af.mil; Tel: +1 937 255 6825*
[d] *Department of Physics and Astronomy, University of Southern Mississippi, Hattiesburg, MS 39406, USA. E-mail: ras.pandey@usm.edu; Fax: +1 601 266 5149; Tel: +1 601 266 4485*

† Electronic supplementary information (ESI) available: Larger snapshot images at $t = 10^5$ and 10^6 for simulations containing peptide concentrations 0.01, 0.02, 0.03, 0.05, and 0.07. See DOI: 10.1039/c0cp01364a

1A peptide (from the frustle of the diatom *Cylindrotheca fusiformis*) and dynamic light scattering analysis on polyamines demonstrated that these silica-forming molecules are not monomeric in solution and form aggregates.[6,10,11,13] Other studies suggest that self-assembly is required for biosilica formation, as it provides a structure-specific template for rapid silicic acid poly-condensation or forms microemulsions that act as flocculating agents to promote silica aggregation and precipitation *via* a phase separation mechanism.[12,15,16] In a seminal study by Kröger *et al.*, dephosphorylated silaffins did not self-assemble and thus, had lost the ability to biomineralize silica.[7] The addition of phosphate ions restores silica formation by allowing the positively-charged peptides to self-assemble *via* intermolecular phosphate anion bridges. Likewise, the unphosphorylated peptides that mimic silaffins require the addition of phosphate to catalyze silica formation. Understanding the mechanism of self-assembly prior to silica condensation is the first step in synthesizing complex silica structures at the molecular level.

The antimicrobial peptide KSL (KKVVFKVKFK) is a pertinent example of a peptide that catalyzes fortuitous biomineralizations reactions.[17] KSL will promote silica precipitation and form silica nanoparticles when added to solutions containing phosphate buffer (pH = 8) and hydrolyzed tetramethyl orthosilicate (TMOS). The sequence of KSL is rich in lysines that are interspersed with the hydrophobic amino acids, valine and phenylalanine. In addition to its biomineralization properties, KSL is a potent antimicrobial agent. The sequence endows the peptide with specific ionic and hydrophobic properties that imparts biocidal activity toward a wide range of microorganisms.[18] Cationicity and amphiphilicity are inherent to many antimicrobial peptides (AMPs) and several models suggest that AMPs will self-assemble into supramolecular structures within microbial cell membranes and disrupt their integrity and function.[18,19] While the antimicrobial activity and biomineralization properties of KSL are likely coincidental, we propose that the self-organization due to cationic and amphiphilic properties of KSL also mediates rapid silica condensation.

Monte Carlo-led lattice simulations have been extensively used to describe the aggregation properties of proteins and small peptides in amyloid and prion diseases,[20,21] interactions between AMPs and cellular membranes,[22,23] and bio-inorganic interactions that occur in peptide-mediated biomineralization reactions.[24–28] Generic aspects of oligomerization and patterned assembly can be gleaned from simulations that provide simplified protein models based on relevant properties of protein–protein or protein–solvent interactions and computational algorithms that rely on repeated random sampling of stochastic motion. In a previous study, Lenoci and Camp have analyzed the self-assembly of silaffins peptides with long-chain polyamines by a coarse-grained computer simulation model.[24] Using an attenuated description of polyamine tails on the native silaffin 1A protein, the self-organization of peptides was successfully captured by coarse-grained interactions among different components. The Lenoci and Camp model varied the concentration of the peptide fragment and studied its aggregation leading to scaffolds (clusters) and complementary pore spaces (cavities). The peptide clusters are isolated with open pores at low concentration and large connected clusters with confined cavities at higher concentrations. The results suggest that self-assembled structures act as either nucleation points or scaffolds for the deposition of silica.

In our study, we consider the first computational model to understand the self-organization of a biomineralizing peptide in the presence of an ionic solution. Unlike the study by Lenoci and Camp, we retain the electrostatic and hydrophobic properties of each amino acid and incorporate explicit solvent to represent phosphate. While the structural details of each amino acid are ignored, the model incorporates the specific strength of every possible interaction between two different amino acids, based upon a database of known interactions (see below). Because of the efficiency of the bond-fluctuation model[29,30] with ample degrees of freedom on a discrete lattice, we are able to explore a relatively larger phase space by the Monte Carlo simulations to study the self-organizing structural evolution with a range of interaction strengths between phosphate and lysine. We examine a number of local and physical quantities. The results provide insight into the self-organizing behavior of short, amphipathic peptides in biological systems and in nanomaterials synthesis.

2. Model

A coarse-grained description for KSL is used to examine the self-organizing structures in the presence and absence of phosphate on a three dimensional discrete (cubic) lattice.[26,31] An amino acid residue is represented by a particle or node. Therefore, the peptide is composed of a set of nodes tethered together in a flexible chain in a specific sequence. KSL is a chain of ten amino acids: five lysines (Lys, K), three valines (Val, V), and two phenylalanines (Phe, F), in the specific sequence, KKVVFKVKFK. The peptide chain with the covalently bonded nodes is represented by the bond-fluctuation model on a lattice with a cubic grid.[29] A node is represented by a unit cube (occupying its eight lattice sites) and the bond length between consecutive nodes can fluctuate between 2 and $\sqrt{10}$ with an exception of $\sqrt{8}$ in unit of lattice constant. Such a bond-fluctuation description is known to capture the computational efficiency while incorporating ample degrees of freedom in complex polymer systems, peptides, and multi-component nanocomposites.[26,29,31,32] The phosphate constituent is represented by a particle with the same size as that of a residue node.

The simulation box consists of peptides and phosphate constituents with concentration C_{KSL} and C_{Ph}, respectively. Apart from excluded volume constraints, each residue and phosphate constituent interact with a pair potential. The interaction strength between two elements at sites i and j separated by a distance r_{ij} is represented by the Lennard–Jones (LJ) potential:

$$U_{ij} = f\left[|\varepsilon_{ij}|\left(\frac{\sigma}{r_{ij}}\right)^{12} + \varepsilon_{ij}\left(\frac{\sigma}{r_{ij}}\right)^{6}\right], \quad r_{ij} < r_c$$

where r_c ($=\sqrt{8}$) is the interaction cut-off range and $\sigma = 1$ in unit of lattice constant. The strength of the interaction $f\varepsilon_{ij}$ is controlled by an arbitrary parameter f ($f > 0$) that can be

varied with positive (repulsive) and negative (attractive) parameter ε_{ij} characteristics of each constituent (see below). The distance between two sites is discrete and measured in lattice constant units. The depth of the LJ potential is controlled by the magnitude of the pair interaction strength $f\varepsilon_{ij}$ in Boltzmann constant units. The interaction matrix could be relatively large for large peptides. Since only three different amino acid residues (K, V, F) comprise KSL, the interaction matrix is relatively small. The number of the pair interaction matrix elements is further reduced due to symmetries (*e.g.*, $\varepsilon_{ij} = \varepsilon_{ji}$). The magnitude of each interaction element (ε_{ij}) is based on the insight gained from all atomistic description and general characteristics.[26] To capture the specificity, every possible interaction between two different amino acids is considered. The interaction strength of each residue–residue contact is based on a table of inter-residue contact energies derived from a set of known residue interactions in the Protein Data Bank. In this study by Miyazawa and Jernigan,[33] inter-residue contact energies for all pairs of amino acids were calculated empirically by quantifying and averaging all residue–residue contacts ($N_{rr} > 18\,000$) identified in a set of globular protein crystal structures. Based on the assumption that the native conformations of proteins reflect the lowest free energy of residue–residue interactions, the average of all inter-residue contacts found in the population of protein structures was used to formulate a relative table of intrinsic interaction strengths for all amino acid pairs.

In KSL, most residues are lysine (K) and are positively charged, while the remaining residues are phenylalanine (F) and valine (V) and are both hydrophobic. Based on the inter-residue contact energies established by Miyazawa and Jernigan,[33] the interactions among hydrophobic groups are attractive and their interaction strengths are: $\varepsilon_{VF} = -0.22$, $\varepsilon_{VV} = -0.29$, and $\varepsilon_{FF} = -0.44$. Interactions between lysines are repulsive ($\varepsilon_{KK} = +0.25$), as are the interactions between lysine and the hydrophobic residues ($\varepsilon_{VK} = \varepsilon_{FK} = +0.44$). The interactions between lysine and phosphate are more attractive and are varied in simulations ($\varepsilon_{KPh} = -0.5$ to -0.8). The interaction strength between lysine and phosphate is varied because an intrinsic energy of this pair was not determined in the Miyazawa and Jernigan study.[33] Accordingly, we choose a range that is within the range of contact energies calculated between oppositely-charged amino acids (*i.e.*, aspartic and glutamic acid *vs.* lysine, arginine, and histidine), which ranged from approximately -0.4 to -1.0. Phosphate buffer at physiological conditions is mostly either $H_2PO_4^-$ or HPO_4^{-2}, and the polyionic nature of these species invokes transient bonding with each other, so phosphate–phosphate interactions are assigned as weakly attractive ($\varepsilon_{PhPh} = -0.1$). The arbitrary parameter f can be selected to accentuate the differences in dependence of the physical quantities on the peptide concentration; we choose $f = 100$ here. The reduced temperature $T = 1$ in unit of the Boltzmann constant.

Each simulation is initiated with a random distribution of peptide chains and phosphate particles on a cubic lattice (L^3). The Metropolis algorithm is used to stochastically select and move each peptide node and phosphate particle. A peptide node or phosphate particle at a site i and one of its neighboring site j are selected randomly. If the neighboring site j is empty and the selected constituent at site i is a phosphate particle, then an attempt is made to move the phosphate from site i to site j with the Boltzmann probability $e^{-\Delta E/T}$, where $\Delta E = E_j - E_i$ is the change in energy as a result of the move and T is the temperature in Boltzmann constant units. If the selected constituent is a peptide node, then the bond-fluctuation constraint is implemented in addition to Boltzmann probability for its move from site i to site j. A time step (t) is defined as an attempt to move each residue and phosphate particle once (*i.e.*, Monte Carlo step or MCS).

Simulations with KSL were first performed in the absence of phosphate. A series of simulations were then carried out with varying volume fractions of peptide chains ($C_{KSL} = 0.01$–0.07) with a constant phosphate particle volume fraction ($C_{Ph} = 0.1$) for a range of interaction strengths between lysine and phosphate. In laboratory experiments, the molar ratio between phosphate and KSL is much higher than in our simulations ($\sim 10^5$). In order to study peptide aggregation and scaffolding, an ample number of KSL chains is required in the lattice, in order to provide a sufficient number of peptide interactions for meaningful analysis. At experimental molar ratios, the simulation would not contain an adequate number of peptide constituents. To overcome the deficiency, more peptide chains can be included in a larger lattice (*e.g.*, 128^3 or greater) and simulation times extended to allow the peptides to interact and reach equilibrium. Unfortunately, the required increase in lattice space and/or time steps to accommodate experimental conditions is constrained by computing hardware, resources, and time. After running several test simulations at different lattice sizes (64^3 and 128^3) and different time steps ($t = 10^5$ and 10^6 MCS), ultimately, a lattice size of 64^3 and a time step length of $t = 10^6$ were selected for simulations in the study. We did not observe significant differences in peptide dynamics between simulations using different lattice sizes, but did notice that simulations required $> 10^5$ time steps to reach equilibrium (Fig. S1 of the ESI†). Results are an average of 10–50 independent simulations for each sample condition. Under these conditions, the consolidated results were sufficient to calculate the average values of a range of local and global physical quantities and show clear trends between the different simulation conditions.

3. Results and discussion

3.1 Self-assembly of peptide in the absence and presence of phosphate

The final snapshots (*i.e.*, at the end of million time steps) of simulations containing peptide in the absence and presence of phosphate are presented in Fig. 1. In the absence of phosphate, a minimal amount of peptide aggregation is observed, particularly at the larger C_{KSL} concentrations. As the only attractive forces in these simulations, it is likely that the hydrophobic residues interact and cause the peptides to relax into small aggregates. The peptide chains exhibit mostly random conformations, although a few are shown folded upon themselves. There is a greater probability that hydrophobic residues on the same peptide will interact first, resulting in the folded conformation.

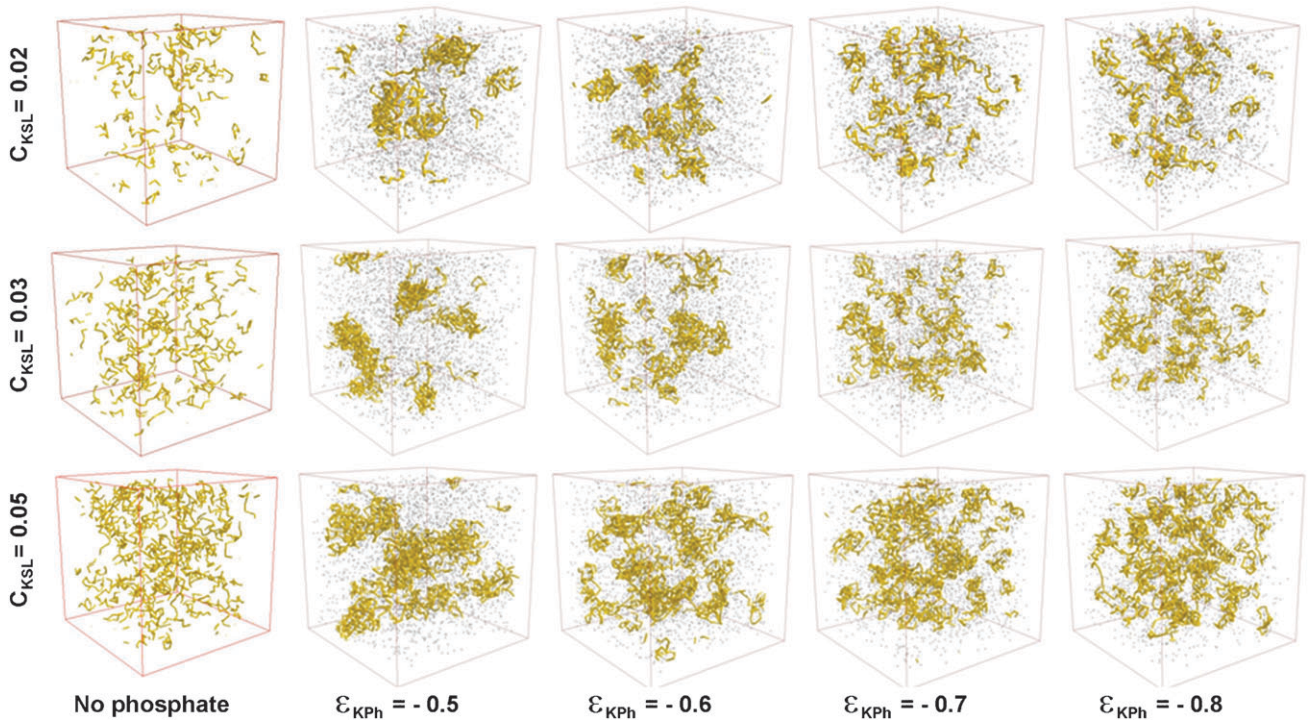

Fig. 1 Final snapshots ($t = 10^6$ MCS) for simulations of increasing peptide concentration (C_{KSL}, rows top to bottom) and increasing lysine–phosphate interaction strength (ε_{KPh}, second column from left to right). First column on left is final snapshots of simulations without phosphate. All snapshots (including $C_{KSL} = 0.01$ and 0.07) are provided as larger figures in Fig. S2 of the ESI.†

In simulations containing phosphate, the images clearly show that phosphate molecules induce peptide to organize into clusters. Large aggregates are observed in snapshots at the lowest lysine–phosphate interaction strength ($\varepsilon_{KPh} = -0.5$). Surprisingly, increasing the ε_{KPh} appears to disrupt the local density of the large aggregates, rather than causing increased density and further expansion of large aggregates. The size of the aggregate particles decreases and the network of peptides also spreads or fractionates into smaller complexes. The competition between the residue–residue and phosphate–lysine interaction leads to distinct assemblies of aggregates as a function of interaction strength. At low ε_{KPh}, hydrophobic interactions play a role in aggregation kinetics and yield one type of aggregate morphology. At high ε_{KPh}, it appears that phosphate–lysine interactions overcome the hydrophobic interaction strength, which results in a different aggregate structure. This assessment is based on visual interpretation of the simulation snapshots; in the following sections, we determine the quantitative structural correlations.

3.2 Local structural correlations

Correlation between local structure and the number of interactions between different constituents is determined by calculating the average number of hydrophobic residues (N_H) and phosphates (N_{Ph}) within the range of interaction ($r = \sqrt{8}$) of each residue. In simulations containing $C_{KSL} = 0.03$ and 0.05,‡ we see at $\varepsilon_{KPh} = -0.5$, the hydrophobic residues of KSL (V_3, V_4, F_5, V_7, and F_9) contain the highest number of hydrophobic interactions (Fig. 2A). As ε_{KPh} increases, N_H of the hydrophobic residues decreases, while the N_H around lysine residues (K_1, K_2, K_6, K_8, and K_{10}) remains relatively the same. The opposite trend is true when we calculate the average number of phosphates (N_{Ph}) within the range of interaction around each residue (Fig. 2B). As ε_{KPh} increases, the number of phosphate interacting with lysine increases, while the number of phosphates surrounding the hydrophobic residues remains relatively constant. This trend can be further clarified by plotting the average number of hydrophobic residues and phosphates within the range of interaction for each residue as a function of ε_{KPh} (Fig. 3). At low ε_{KPh}, hydrophobic interactions (labeled (a) in Fig. 3) are nearly as numerous as lysine–phosphate interactions (b). As ε_{KPh} increases, phosphate–lysine interactions dominate and consequently, N_H of Val and Phe decreases (c). Concurrently, the number of phosphates interacting with the peptide increases (d). Here, it is clear that the aggregation properties at low ε_{KPh} are influenced by hydrophobic interactions and at larger ε_{KPh}, phosphate percolates into the clusters and re-organizes the peptide molecules to form new clusters of a smaller size and lower local peptide density.

3.3 Distribution of constituents within peptide aggregates

Although the local structural correlations discussed above are insightful, it does not provide the overall structure of the whole system. To gain insight into the spatial distribution of substituents throughout the entire lattice, the radial distribution function (*rdf*) can be used to correlate the global structure of the system. In our simulations, the *rdf* measures how the density of residues and phosphates changes as a function of

‡ Unless otherwise shown, results from simulations containing $C_{KSL} = 0.03$ and 0.05 were representative of simulations at all C_{KSL}.

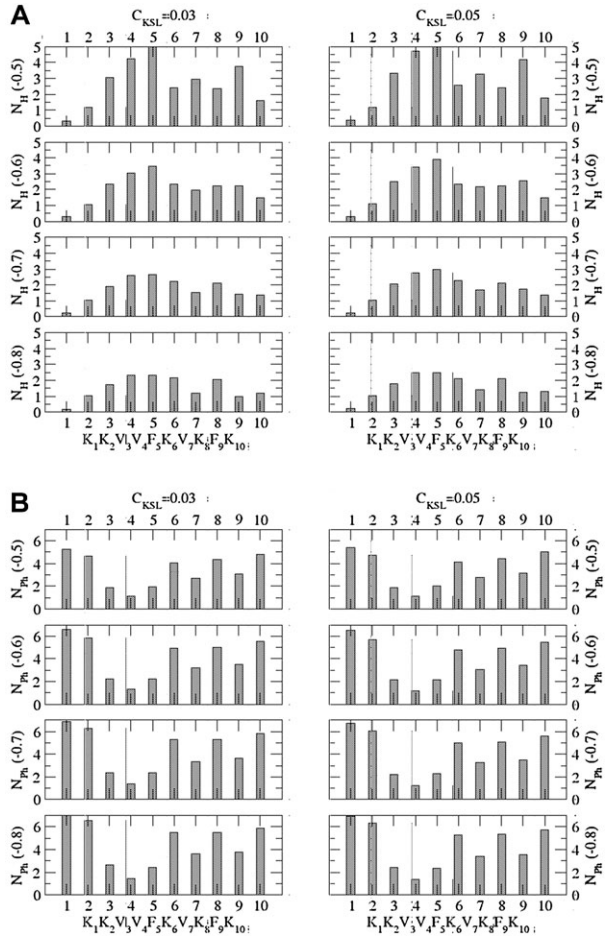

Fig. 2 The average number of hydrophobic residues (A) and phosphates (B) around each residue. Peptide concentrations in simulations (C_{KSL}) are 0.03 (left) and 0.05 (right) and the lysine–phosphate interaction strength (ε_{KPh}) for each bar graph is shown in parentheses. Each residue is represented by a number (shown at bottom).

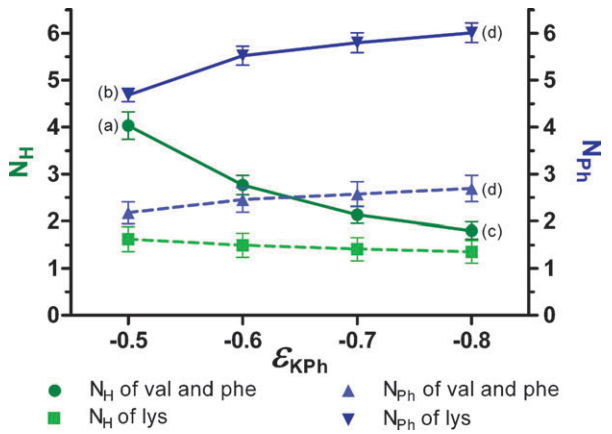

Fig. 3 Average change in N_H and N_{Ph} for hydrophobic residues and lysines as a function of ε_{KPh}. Letter designations (a–d) are described in the text. Simulation conditions are the same as described in Fig. 2 and error bars show standard error of the mean.

the distance from each substituent (residue or phosphate). The number of lattice sites either occupied by a residue or a phosphate (N_1) is counted between two concentric spheres having radii r_1 and r_2 (where $r_2 > r_1$) measured from each substituent. The average density $\rho(r)$ of this region is N_1/N, where N is the total number of lattice sites (empty or occupied) between r_1 and r_2. We can evaluate $\rho(r)$ around each residue within a range of r lying between r_1 and r_2 while keeping Δr sufficiently small and estimate the average (*i.e.*, *rdf*). We have used r^2 = 1–100, which allows the function to extend further than the local structural correlation and gauge the distribution of different components throughout the aggregates.

Fig. 4 shows the *rdf* as a function of radial distance r for all residues and phosphates at $t = 10^6$ in simulations where C_{KSL} = 0.03 and 0.05. For each ε_{KPh} in simulations with phosphate, it is apparent that residues are concentrated at set intervals as the radial distance is increased from each residue (A). This suggests that peptides are uniformly patterned within the composite. A similar distribution is also observed when the *rdf* of phosphate is plotted as a function of r (B). When the *rdf* of residues and phosphates for each r are compared, the results demonstrate that the aggregates are organized as alternating phosphates and peptides. For each concentrated distribution of residues at a radial distance r, there is a corresponding drop in phosphate groups and *vice versa*. This alternating trend is observed in simulations through the entire range of ε_{KPh}. The findings confirm that the aggregates are formed through peptide molecules interconnected *via* phosphate bridges. The patterning of peptides within the aggregates is mediated by phosphate, because this unique distribution of residues is not

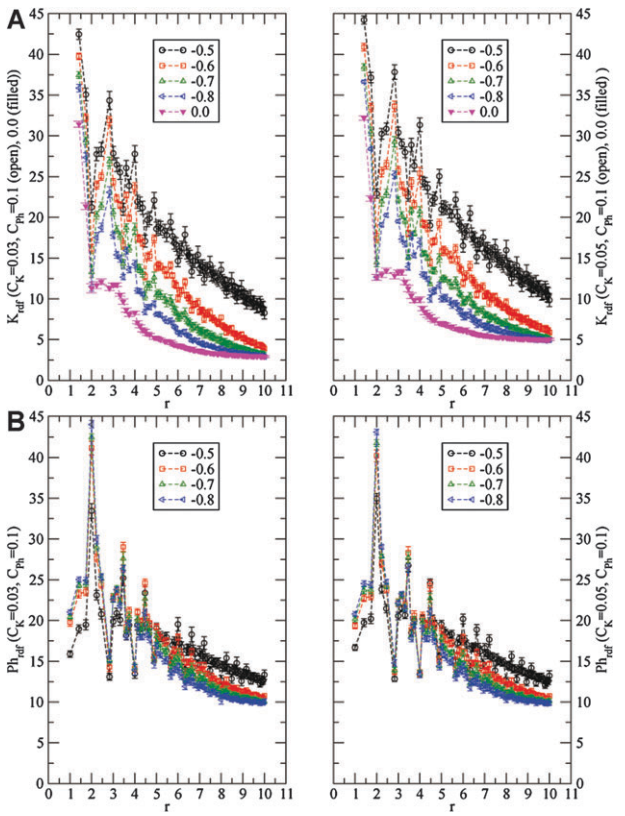

Fig. 4 The *rdf* for all residues (A) and for phosphates (B) for simulations where the peptide concentration (C_{KSL}) is 0.03 (left) and 0.05 (right). The legend (inset) lists ε_{KPh}. The *rdf* plotted for all residues in simulations without phosphate is listed in the legend as 0.0.

observed in the absence of phosphate (inverted, filled triangles in top row of graphs).

3.4 Peptide mobility and conformation

We examined the mobility of each residue by monitoring its movement throughout the simulation. Residue mobility is defined as the number of successful moves per unit time step MCS. Fig. 5 shows the mobility profile of KSL by measuring the number of successful moves of each residue in the absence and presence of phosphate and over each ε_{KPh}. The mobility of residues is much higher in the absence of phosphate. The residues at the end of the peptide chains (*i.e.*, K_1 and K_{10}) are much more mobile than the interior residues as one would expect from the segmental dynamics of a chain. The mobility of interior residues is nearly three times lower than the end residues but still much higher than the corresponding residues in the presence of phosphate. A different mobility profile is recorded for peptide in the presence of phosphate. In general, the mobility of each lysine is lower relative to the hydrophobic residues mobility. We see that the mobility of each lysine residue decreases monotonically on increasing ε_{KPh}. The mobility of lysine decreases over increasing ε_{KPh} due to its selective binding with the phosphate. Phosphate is thus critical in orchestrating the mobility of each residue and therefore attributes its structural characteristics in a specific sequence of KSL.

We also examined the conformation of individual peptide chains as they self-assemble in the absence and presence of phosphate by calculating the radius of gyration (R_g) and end-to-end distance (R_e) of peptide chains over time (Fig. 6). It is apparent that the peptide chains remain stretched out in the absence of phosphate and contract when phosphate is added to the simulation. A large change in peptide conformation occurs if the interaction strength between lysine and phosphate is changed from −0.5 to −0.6. At $\varepsilon_{KPh} = -0.5$, peptides slowly condense into small structures and do not reach an equilibrium at the last time step, while in simulations where $\varepsilon_{KPh} \geq -0.6$, peptides in the presence of phosphate form an energy-minimized conformation more rapidly. The final energy-minimized conformation is about one-third smaller than the peptide in its fully extended and freely mobile state.

A reduction in R_g and R_e further demonstrates that the peptides aggregate and are either compacted by lysine–phosphate interactions or fold upon themselves *via* multiple interactions between a single phosphate and more than one lysine from the same peptide. Both of these interactions are observed in final snapshots (Fig. 1 and Fig. S2 of the ESI†). A reduction in R_g and R_e did not occur in the absence of phosphate, even though we did observe that a few peptides are folded and condensed in final snapshots of these simulations. Apparently, these types of peptide conformations are not stable in the absence of phosphate, and repulsive interactions between lysines and between hydrophilic and hydrophobic residues compete with attractive hydrophobic interactions to maintain random conformations of mostly extended peptides throughout the simulation.

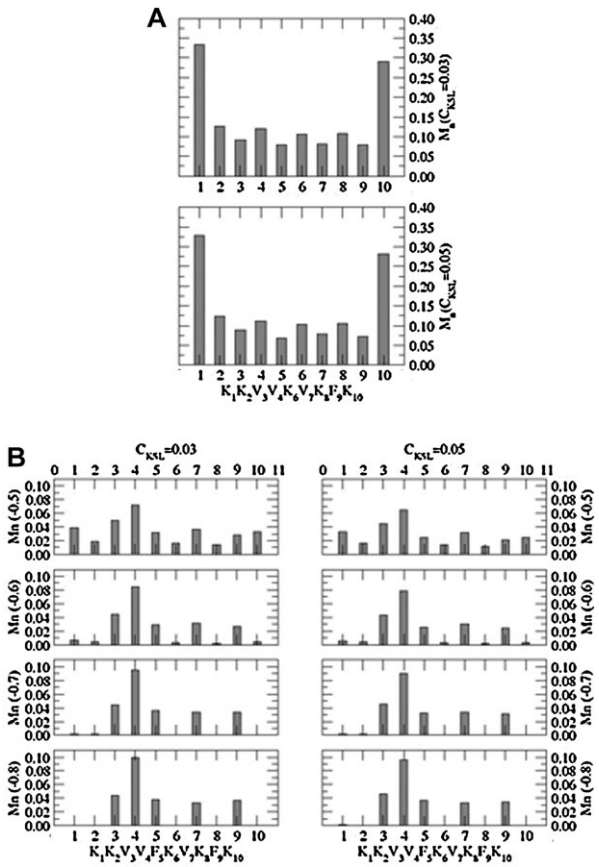

Fig. 5 The average mobility of each residue in the absence of phosphate (A) and in the presence of phosphate (B). In (A), C_{KSL} in simulations are 0.03 (top graph) and 0.05 (bottom graph). In (B), the C_{KSL} are 0.03 (left) and 0.05 (right) and ε_{KPh} for each bar graph is shown in parentheses. Each residue is represented by a number (shown at bottom).

4. Summary and conclusions

A coarse-grained model was used to study the self-organizing behavior of an antimicrobial peptide (KSL) and phosphate. Specificity of each residue and their interactions with each other and phosphate was considered in simulations. Each

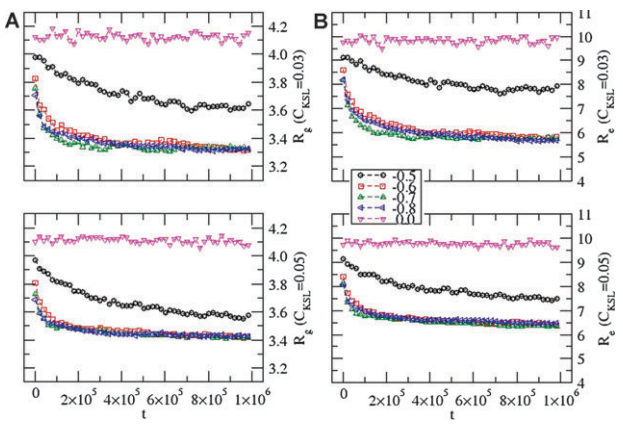

Fig. 6 Peptide chain radius of gyration (A) and end-to-end distance (B) for C_{KSL} = 0.03 (top) and C_{KSL} = 0.05 (bottom). The interaction strength of each simulation is listed in the legend (inset). Simulations in the absence of phosphate are listed as 0.0.

component was allowed to execute its stochastic motion *via* the Metropolis algorithm. Both local and global physical quantities were monitored during the course of simulations. The local quantities were mobility profiles of each residue and their characteristic neighborhood within the range of interaction. The global quantities included the radial distribution function (*rdf*), the radius of gyration (R_g) and end-to-end distance (R_e) of peptide chains.

We find that peptide assembly into scaffold structures is mediated by phosphate. Upon assembly, the peptides and phosphates segregate and form composite aggregates. The simulations reveal that when assuming stronger interactions between peptide and phosphate, the mobility of lysine residues decreases, while the average number of surrounding phosphate within the range of interactions increases. Thermodynamic equilibration directs phosphate constituents to mobilize around lysine residues, recruiting peptides to form composite aggregates involving scaffolds. Monitoring the R_g and R_e of peptides over time in simulations where $\varepsilon_{KPh} > -0.5$ reveals that the local peptide structure condenses relatively quickly. At higher ε_{KPh}, most of the phosphates become strongly mobilized around lysine, resulting in a compact conformation of the peptide. As shown by the antagonistic fluctuations of the residue and phosphate *rdf* as a function of radial distance *r*, the equilibrated state is an ordered assembly of peptide residues interspersed with phosphate.

The specific ordered arrangement of phosphate and KSL is an intriguing result and reflects several proposed mechanisms addressing the molecular self-assembly of biosilicifying polymers. Phosphate-bridging mechanisms have been proposed to explain the aggregation of peptides and polyamine chains prior to inducing silica formation.[6,7,11,34,35] The polyionic structure of phosphate facilitates bonding to multiple peptides and the cross-linking required to build supramolecular structures of aggregated peptide. Phosphate cross-linking of biomolecules prior to silica condensation has been shown in poly-L-lysine supramolecular assemblies,[34,35] poly(allylamine) aggregates,[11] and naturally-occurring LCPA scaffolds.[36] In the biomineralization of silica, it is hypothesized that the coordination of phosphate and peptide may induce a conformational shift to spatially or electrostatically orient functional groups to bind and react with silicate species. This has been proposed in silicification reactions using non-peptidyl polyamines[13,37,38] and may likely occur in similar reactions with amine-rich polypeptides. The results of our simulations, which demonstrate a highly ordered assembly of peptide in the presence of phosphate, are consistent with proposed models of supramolecular polyamine and peptide assemblies that act as silica template.

The phosphate bridging interactions observed in our simulations also reflect the proposed mechanisms of *in vitro* silaffin self-assembly prior to silica deposition.[6,7] The self-assembly of native silaffin peptide fragments is mediated by intermolecular interactions between the cationic polyamine chains on lysines and anionic phosphoryl modifications on serines. When the peptide is synthesized without any modifications (SSKKSGSYSGSKGSKRRIL, known as the R5 peptide), assembly into aggregates is induced in the presence of phosphate buffer. Without the phosphoryl groups on the serines of the R5 peptide, phosphate buffer is required for self-assembly. If the serines are present in the R5 peptide sequence solely to tether phosphate molecules and the intrinsic properties of the serine residues are not directly involved in self-assembly, the remaining sequence of R5 (KKGYGKGKRRIL) shares significant identity and arrangement to KSL, except for the C-terminal RRIL residues. While the RRIL motif has shown to control assembly of R5 into large aggregates, it is not essential, because the same peptide without the RRIL motif (SSKKSGSYSGSK) also induces the formation of active silica precipitating assemblies.[39] Considering the sequence of cationic and hydrophobic residues on the R5 peptide is nearly identical to KSL, it would not be surprising if these two peptides share similar assembly mechanisms. Similar modeling studies using the R5 peptide are underway and comparison between R5 and KSL may assist in a better understanding of the fundamental mechanisms that drive peptide self-assembly.

Our coarse-grained model is able to characterize the structural properties of peptide assemblies that result from residue-specific interactions and also global dynamics of the system, because of the assimilation of the intra-residue details in a single peptide node. In contrast, simulations that define the atomic structure of each residue of KSL and phosphate would limit the number of constituents and time scales necessary for ordered aggregates to form and therefore cannot accurately define all structural dynamics of the complete system. Though to identify the molecular structure and electronic state of peptide–phosphate templates that induce silica condensation, atomistic simulations are required to characterize the specific coordination chemistry between functional groups of amino acids and phosphate. Subsequent work will build upon the simulation model presented here and more accurately define the atomic structures of KSL and phosphate and also survey additional biomineralizing peptides in different ionic solvents to reveal how different sequences of amino acids interact to form specific supramolecular assemblies. Once a repertoire of interactions has been identified, we can then move forward to design molecular blueprints of complex structures that will mimic the vast diversity of nanostructured materials we find in nature.

Acknowledgements

This work was supported through funding from the Air Force Materials and Manufacturing Directorate (AFRL/RX) and the Joint Science Technology Office of the Defense Threat Reduction Agency, Project Code AA06CBT008 (Ilya Elashvili, Jennifer Becker and Stephen Lee, Program Managers).

References

1 *Silica-Based Materials for Advanced Chemical Applications*, ed. M. Pagliaro, Royal Society of Chemistry, Cambridge, 2009.
2 *Handbook of Biomineralization: Biological Aspects and Structure Formation*, ed. E. Baeuerlein, WILEY-VCH Verlag GmbH & Co., Weinheim, 2007.
3 M. Hildebrand, *Chem. Rev.*, 2008, **108**, 4855–4874.
4 N. Kröger, R. Deutzmann and M. Sumper, *Science*, 1999, **286**, 1129–1132.
5 C. C. Perry and T. Keeling-Tucker, *JBIC, J. Biol. Inorg. Chem.*, 2000, **5**, 537–550.

6 M. Sumper and N. Kröger, *J. Mater. Chem.*, 2004, **14**, 2059–2065.
7 N. Kröger, S. Lorenz, E. Brunner and M. Sumper, *Science*, 2002, **298**, 584–586.
8 P. Behrens, M. Jahns and H. Menzel, in *Handbook of Biomineralization: Biomimetic and Bioinspired Chemistry*, ed. P. Behrens and E. Baeuerlein, WILEY-VCH Verlag GmbH & Co., Weinhein, 2007, pp. 3–18.
9 W. J. Crookes-Goodson, J. M. Slocik and R. R. Naik, *Chem. Soc. Rev.*, 2008, **37**, 2403–2412.
10 E. Brunner, K. Lutz and M. Sumper, *Phys. Chem. Chem. Phys.*, 2004, **6**, 854–857.
11 K. Lutz, C. Groger, M. Sumper and E. Brunner, *Phys. Chem. Chem. Phys.*, 2005, **7**, 2812–2815.
12 S. V. Patwardhan, S. J. Clarson and C. C. Perry, *Chem. Commun.*, 2005, 1113–1121.
13 D. J. Belton, S. V. Patwardhan, V. V. Annenkov, E. N. Danilovtseva and C. C. Perry, *Proc. Natl. Acad. Sci. U. S. A.*, 2008, **105**, 5963–5968.
14 K. M. Delak and N. Sahai, *J. Phys. Chem.*, 2006, **110**, 17819–17829.
15 T. Coradin and P. Lopez, *ChemBioChem*, 2003, **4**, 251–259.
16 M. Sumper, *Science*, 2002, **295**, 2430–2433.
17 D. M. Eby, K. E. Farrington and G. R. Johnson, *Biomacromolecules*, 2008, **9**, 2487–2494.
18 S. Y. Hong, J. E. Oh, M. Kwon, M. J. Choi, J. H. Lee, B. L. Lee, H. M. Moon and K. H. Lee, *Antimicrob. Agents Chemother.*, 1998, **42**, 2534–2541.
19 K. A. Brogden, *Nat. Rev. Microbiol.*, 2005, **3**, 238–250.
20 B. Ma and R. Nussinov, *Curr. Opin. Chem. Biol.*, 2006, **10**, 445–452.
21 E. Małolepsza, M. Boniecki, A. Kolinski and L. Piela, *Proc. Natl. Acad. Sci. U. S. A.*, 2005, **102**, 7835–7840.
22 P. La Rocca, P. C. Biggin, D. P. Tieleman and M. S. P. Sansom, *Biochim. Biophys. Acta, Biomembr.*, 1999, **1462**, 185–200.
23 D. Shental-Bechor, T. Haliloglu and N. Ben-Tal, *Biophys. J.*, 2007, **93**, 1858–1871.
24 L. Lenoci and P. J. Camp, *J. Am. Chem. Soc.*, 2006, **128**, 10111–10117.
25 L. Lenoci and P. J. Camp, *Langmuir*, 2007, **24**, 217–223.
26 R. B. Pandey, H. Heinz, J. Feng, B. L. Farmer, J. M. Slocik, L. F. Drummy and R. R. Naik, *Phys. Chem. Chem. Phys.*, 2009, **11**, 1989–2001.
27 C. R. So, J. L. Kulp, E. E. Oren, H. Zareie, C. Tamerler, J. S. Evans and M. Sarikaya, *ACS Nano*, 2009, **3**, 1525–1531.
28 M. Yang, P. M. Rodger, J. H. Harding and S. L. S. Stipp, *Mol. Simul.*, 2009, **35**, 547–553.
29 *Monte Carlo and Molecular Dynamics Simulations in Polymer Science*, ed. K. Binder, Oxford University Press Inc., New York, 1995.
30 I. Carmesin and K. Kremer, *Macromolecules*, 1988, **21**, 2819–2823.
31 R. B. Pandey and B. L. Farmer, *J. Chem. Phys.*, 2009, **130**, 044906.
32 R. B. Pandey and B. L. Farmer, *J. Polym. Sci., Part B: Polym. Phys.*, 2008, **46**, 2696–2710.
33 S. Miyazawa and R. L. Jernigan, *Macromolecules*, 1985, **18**, 534–552.
34 H. Cui, V. Krikorian, J. Thompson, A. P. Nowak, T. J. Deming and D. J. Pochan, *Macromolecules*, 2005, **38**, 7371–7377.
35 M. M. Tomczak, D. D. Glawe, L. F. Drummy, C. G. Lawrence, M. O. Stone, C. C. Perry, D. J. Pochan, T. J. Deming and R. R. Naik, *J. Am. Chem. Soc.*, 2005, **127**, 12577–12582.
36 M. Sumper, S. Lorenz and E. Brunner, *Angew. Chem., Int. Ed.*, 2003, **42**, 5192–5195.
37 D. Belton, S. V. Patwardhan and C. C. Perry, *Chem. Commun.*, 2005, 3475–3477.
38 D. Belton, S. V. Patwardhan and C. C. Perry, *J. Mater. Chem.*, 2005, **15**, 4629–4638.
39 M. R. Knecht and D. W. Wright, *Chem. Commun.*, 2003, 3038–3039.